

1 **Title:**

2 Isolation of an archaeon at the prokaryote-eukaryote interface

3

4 **Authors:**

5 Hiroyuki Imachi^{1*}, Masaru K. Nobu^{2*}, Nozomi Nakahara^{1,3}, Yuki Morono⁴, Miyuki
6 Ogawara¹, Yoshihiro Takaki¹, Yoshinori Takano⁵, Katsuyuki Uematsu⁶, Tetsuro Ikuta⁷,
7 Motoo Ito⁴, Yohei Matsui⁸, Masayuki Miyazaki¹, Kazuyoshi Murata⁹, Yumi Saito¹, Sanae
8 Sakai¹, Chihong Song⁹, Eiji Tasumi¹, Yuko Yamanaka¹, Takashi Yamaguchi³, Yoichi
9 Kamagata², Hideyuki Tamaki² and Ken Takai¹

10

11 *These authors contributed equally to this work.

12

13 **Affiliations:**

14 ¹Institute for Extra-cutting-edge Science and Technology Avant-garde Research (X-star),
15 Japan Agency for Marine-Earth Science and Technology (JAMSTEC), Yokosuka, Japan

16 ²Bioproduction Research Institute, National Institute of Advanced Industrial Science and
17 Technology (AIST), Tsukuba, Japan

18 ³Department of Civil and Environmental Engineering, Nagaoka University of
19 Technology, Nagaoka, Japan

20 ⁴Kochi Institute for Core Sample Research, X-star, JAMSTEC, Nankoku, Japan

21 ⁵Biogeochemistry Program, Research Institute for Marine Resources Utilization,
22 JAMSTEC, Yokosuka, Japan

23 ⁶Department of Marine and Earth Sciences, Marine Work Japan Ltd, Yokosuka, Japan

24 ⁷Research Institute for Global Change, JAMSTEC, Yokosuka, Japan

25 ⁸Research Institute for Marine Resources Utilization, JAMSTEC, Yokosuka, Japan

26 ⁹National Institute for Physiological Sciences, Okazaki, Japan

27

28 **Corresponding authors:**

29 Hiroyuki Imachi, E-mail: imachi@jamstec.go.jp

30 Masaru K. Nobu, E-mail: m.nobu@aist.go.jp

31

32

33

34 **Abstract**

35 The origin of eukaryotes remains enigmatic. Current data suggests that eukaryotes may
36 have risen from an archaeal lineage known as “Asgard archaea”. Despite the eukaryote-
37 like genomic features found in these archaea, the evolutionary transition from archaea to
38 eukaryotes remains unclear due to the lack of cultured representatives and corresponding
39 physiological insight. Here we report the decade-long isolation of a Lokiarchaeota-related
40 Asgard archaeon from deep marine sediment. The archaeon, “*Candidatus*
41 *Prometheoarchaeum syntrophicum* strain MK-D1”, is an anaerobic, extremely slow-
42 growing, small cocci (~550 nm), that degrades amino acids through syntropy. Although
43 eukaryote-like intracellular complexities have been proposed for Asgard archaea, the
44 isolate has no visible organella-like structure. *Ca. P. syntrophicum* instead displays
45 morphological complexity – unique long, and often, branching protrusions. Based on
46 cultivation and genomics, we propose an “Entangle-Engulf-Enslave (E³) model” for
47 eukaryogenesis through archaea-alphaproteobacteria symbiosis mediated by the physical
48 complexities and metabolic dependency of the hosting archaeon.

49

50 How did the first eukaryotic cell emerge? So far, among various competing evolutionary
51 models, the most widely accepted are the symbiogenetic models in which an archaeal
52 host cell and an alphaproteobacterial endosymbiont merged to become the first eukaryotic
53 cell¹⁻⁴. Recent metagenomic discovery of Lokiarchaeota (and the Asgard archaea
54 superphylum) led to the theory that eukaryotes originated from an archaeon closely
55 related to Asgard archaea^{5,6}. The Asgard archaea genomes encode a repertory of proteins
56 hitherto only found in *Eukarya* (eukaryotic signature proteins – ESPs), including those
57 involved in membrane trafficking, vesicle formation/transportation, ubiquitin and
58 cytoskeleton formation⁶. Subsequent metagenomic studies have suggested that Asgard
59 archaea have a wide variety of physiological properties, including hydrogen-dependent
60 anaerobic autotrophy⁷, peptide or short-chain hydrocarbon-dependent organotrophy⁸⁻¹¹
61 and rhodopsin-based phototrophy^{12,13}. A recent study suggests that an ancient Asgard
62 archaea degraded organic substances and syntrophically handed off reducing equivalents
63 (e.g., hydrogen and electrons) to a bacterial partner, and further proposes a symbiogenetic
64 model for the origin of eukaryotes based on this interaction¹⁴. However, at present, no
65 single representative of the Asgard archaea has been cultivated and, thus, the physiology
66 and cell biology of this clade remains unclear. In an effort to close this knowledge gap,

67 we successfully isolated the first Asgard archaeon and here report the physiological
68 characteristics, potentially key insights into the evolution of eukaryotes.
69

70 **Isolation of an Asgard archaeon**

71 Setting out to isolate uncultivated deep marine sediment microorganisms, we engineered
72 and operated a methane-fed continuous-flow bioreactor system for over 2000 days to
73 enrich such organisms from anaerobic marine methane-seep sediments¹⁵ (Supplementary
74 Text 1). We successfully enriched many phylogenetically diverse yet-to-be cultured
75 microorganisms, including Asgard archaea members (Loki-, Heimdall- and
76 Odinarchaeota)¹⁵. For further enrichment and isolation, sample of the bioreactor
77 community was inoculated in glass tubes with simple substrates and basal media. After
78 approximately one year, we found faint cell turbidity in a Casamino acids-fed culture
79 supplemented with four bacteria-suppressing antibiotics (*i.e.*, ampicillin, kanamycin,
80 streptomycin, and vancomycin; Supplementary Text 2) and incubated at 20°C. Clone
81 library-based small subunit (SSU) rRNA gene analysis revealed a simple community
82 containing many *Halodesulfobacter* and, excitingly, a small population of Lokiarchaeota
83 (Extended Data Table 1). In pursuit of this archaeon, named strain MK-D1, we repeated
84 the subcultures at the time when MK-D1 cell yield was maximized by means of
85 quantitative PCR (qPCR) monitoring. Repeated subcultures gradually enriched the
86 archaeon with extremely slow growth rate and low cell yield (Fig. 1a). The culture
87 consistently had a 30–60 days of lag phase and required over 3 months to reach full
88 growth with a yield of ~10⁵ 16S rRNA gene copies/ml (Fig. 1a). The doubling time was
89 estimated to be approximately 14–25 days. Variation of cultivation temperatures
90 (Extended Data Fig. 1), and substrate combinations and concentrations did not
91 significantly improve the lag phase, growth rate or cell yield (data not shown), while the
92 static cultivation supplemented with 20 amino acids (AAs) and powdered milk resulted
93 in the stable growth. For further characterization, we cultured the archaeon under the
94 optimal conditions determined above.

95 After six transfers, MK-D1 reached 13% abundance in a tri-culture containing
96 *Halodesulfobacter* (85%) and *Methanogenium* (2%) (Extended Data Table 1).
97 Fluorescence *in situ* hybridization (FISH) and scanning electron microscopic (SEM)
98 observation revealed close physical association of the archaeon with the other
99 microorganisms (Figs. 1b–e, Extended Data Fig. 2). Through metagenome-based

100 exploration of this archaeon's metabolic potential and stable isotope probing experiment,
101 we discovered that MK-D1 can catabolize some AAs and peptides through syntrophic
102 growth with *Halodesulfovibrio* and *Methanogenium* via interspecies hydrogen (and/or
103 formate) transfer (Fig. 2 and Supplementary Table S1 and Fig. S1, details in latter
104 section)¹⁶. Indeed, addition of hydrogen scavenger-inhibiting compounds (*i.e.*, 10 mM
105 molybdate and 10 mM 2-bromoethanesulfonate for sulfate-reducing *Halodesulfovibrio*
106 and methanogenic *Methanogenium*, respectively) significantly impeded growth of MK-
107 D1. Through subsequent transfers, we were able to eliminate the *Halodesulfovibrio*
108 population, allowing us to obtain a pure co-culture of the archaeon and *Methanogenium*
109 after a twelve-year journey – starting from deep-sea sediments to a bioreactor-based “pre-
110 enrichment” and a final seven-year *in vitro* enrichment. We here propose the name
111 “*Candidatus* Prometheoarchaeum syntrophicum strain MK-D1” for the isolated
112 Lokiarchaeon.

113

114 **Cell biology and physiology of MK-D1**

115 We further characterized strain MK-D1 using the highly purified cultures and pure co-
116 cultures. Microscopic observations showed that the cells are small cocci, ca. 300–750 nm
117 in diameter (average 550 nm, n=15), and generally form aggregates surrounded with
118 extracellular polysaccharide (EPS)-like materials (Fig. 3a, b and Extended Data Fig. 2),
119 consistent with previous observations using FISH^{15,17}. Dividing cells had less EPS-like
120 materials and a ring-like structure around the middle of cells (Fig. 3c and Extended Data
121 Fig. 2). Cryo-electron and transmission electron microscopic observations revealed that
122 the cells contain no visible organelle-like inclusions (Fig. 3d–f, Extended Data Fig. 2 and
123 Supplementary Movies S1–S3). The cells produce membrane vesicles (MVs; 50–280 nm
124 in diameter) (Fig. 3d–f and Extended Data Fig. 2) and chains of blebs (Fig. 3c and
125 Extended Data Fig. 2e). The cells also form unique membrane-based protrusions with a
126 diameter of about 80–100 nm and various lengths (Fig. 3g–i and Extended Data Fig. 2).
127 Some protrusions remarkably display complex branching, unlike known archaeal
128 protrusions¹⁸. These protrusions were especially abundant after late exponential growth
129 phase. Lipid composition analysis of the MK-D1 and *Methanogenium* co-culture revealed
130 typical archaeal signatures – a C₂₀-phytane and C₄₀-biphytanes (BPs) with 0–2
131 cyclopentane rings (Fig. 3j). Considering the lipid data obtained from a reference

132 *Methanogenium* isolate (99.3% 16S rRNA gene identity; Supplementary Fig. S3), MK-
133 D1 probably contains C₂₀-phytane and C₄₀-BPs with 0–2 rings.

134 MK-D1 can degrade AAs anaerobically, as confirmed by monitoring AAs depletion
135 during the growth of pure co-cultures (Extended Data Fig. 3). We further verify AA
136 utilization by quantifying the uptake of a mixture of ¹³C- and ¹⁵N-labeled AAs through
137 nanometer-scale secondary ion mass spectrometry (NanoSIMS) (Fig. 2b–e). Cell
138 aggregates of MK-D1 incorporated more nitrogen than carbon, suggesting that the
139 possible mixotrophy. Interestingly, the ¹³C-labeling of methane and carbon dioxide varied
140 depending on the methanogenic partner, indicating that MK-D1 produces both hydrogen
141 and formate from AAs for interspecies electron transfer (Extended Data Table 2, see later
142 section). Indeed, addition of high concentrations of hydrogen or formate completely
143 suppressed growth of MK-D1 (Extended Data Table 3). The syntrophic partner was
144 replaceable – MK-D1 could also grow syntrophically with *Methanobacterium* sp. strain
145 MO-MB1¹⁹ instead of *Methanogenium*, which was originally co-enriched with MK-D1
146 (Fig. 2b–e). Although 14 different culture conditions were applied, none of substances
147 (e.g., sugars, electron acceptors, and cell building blocks) enhanced the cell yield,
148 implying specialization to degradation of AAs or peptides (Extended Data Table 3).

149 **Etymology.** *Prometheoarchaeum*, *Prometheus* (Greek): a Greek god who shaped man
150 out of mud and gave them the ability to create fire; *archaeum* from *archaea* (Greek): an
151 ancient life. The genus name is an analogy between this organism's evolutionary
152 relationship with the origin of eukaryotes and the involvement of Prometheus in man's
153 origin from sediments and acquisition of an unprecedented oxygen-driven energy-
154 harnessing ability. The species name, *syntrophicum*, *syn* (Greek): together with; *trephein*
155 (Greek) nourish; *icus* (Latin) pertaining to. The species name referred to syntrophic
156 substrate utilization property of this strain.

157 **Locality.** Isolated from deep-sea methane seep sediment of the Nankai Trough at 2533 m
158 water depth, off Kumano area, Japan.

159 **Diagnosis.** Anaerobic, AA-oxidizing archaeon, small cocci, ca. 550 nm in diameter,
160 syntrophically grows with hydrogen- and formate-utilizing microorganisms. It produces
161 MVs, chains of blebs, and membrane-based protrusions.

162

163

164

165 **Reconstruction of extant and ancestral features**

166 MK-D1 encodes genes for degradation of 10 AAs and reductive generation of H₂ and
167 formate for electron disposal. Most of the identified AA-catabolizing pathways only
168 recover energy through degradation of a 2-oxoacid intermediate (*i.e.*, pyruvate or 2-
169 oxobutyrate; Fig. 2a). MK-D1 can degrade 2-oxoacids hydrolytically (2-oxoacid--
170 formate lyases) or oxidatively (2-oxoacid:ferredoxin oxidoreductases) to yield acyl-CoA
171 intermediates that can be further hydrolyzed for ATP generation. The hydrolytic and
172 oxidative paths release the AA carboxylate group as formate and CO₂ respectively. For
173 the former, formate can be directly handed off to a partnering methanogenic archaea or
174 sulfate-reducing bacteria (SRB). For the latter, reduced ferredoxin generated from 2-
175 oxoacid oxidation can drive reduction of H⁺ to H₂ (electron-confurcating NiFe
176 hydrogenase MvhADG-HdrABC) or CO₂ to formate (formate dehydrogenase FdhA) for
177 interspecies electron transfer. This suggests that MK-D1 has two approaches for
178 syntrophic interaction. A ¹³C-AA-fed co-culture of MK-D1 with *Methanobacterium*
179 generated ¹³C-enriched CH₄ (Extended Data Table 2), indicating syntropy mediated by
180 the hydrolytic path (*i.e.*, AA-derived ¹³C-formate transferred to partner, oxidized to ¹³CO₂,
181 and further reduced to ¹³CH₄). On the other hand, a ¹³C-AA-fed tri-culture of MK-D1
182 with *Halodesulfovibrio* and *Methanogenium* generated ¹³C-enriched CO₂, suggesting the
183 oxidative path (*i.e.*, AA-derived ¹³CO₂ released and mixed with ¹²C-bicarbonate pool in
184 mineral medium). Thus, we confirm that MK-D1 can switch between syntrophic
185 interaction via 2-oxoacid hydrolysis and oxidation depending on the partner(s).

186 The evolutionary relationship between archaea and eukaryotes has been under debate,
187 hinging on the incompleteness and contamination associated with metagenome-derived
188 genomes and variation in results depending on tree construction protocols^{20–23}. By
189 isolating strain MK-D1, we were able to obtain a closed genome (Supplementary Table
190 S1 and Fig. S1) and construct a ribosomal protein-based phylogenomic tree that shows
191 clear phylogenetic sistering between MK-D1 and *Eukarya* (Fig. 4a and Supplementary
192 Tables S4 and S5, and Fig. S4). Thus, strain MK-D1 represents the closest cultured
193 archaeal relative of eukaryotes. We confirmed the presence of many ESPs identified in
194 related Asgard archaea (Supplementary Fig. S5) and obtained the first RNA-based
195 evidence for expression of such genes (Supplementary Table S6).

196 Given the phylogenetic relationship of MK-D1, other Asgard archaea, and eukaryotes,
197 estimating the physiological traits of the last Asgard archaea common ancestor is of

utmost importance. Comparative genomics of MK-D1 and published metagenome-assembled genomes of Asgard archaea revealed that most of the members encode AA-catabolizing pathways, reversible NiFe hydrogenases (MvhADG-HdrABC²⁴ and/or HydAD²⁵) (Fig. 4b), and restricted biosynthetic capacities (*i.e.*, AA and vitamin synthesis; Extended Data Fig. 4), indicating H₂-evolving AA degradation and partner dependence may be a common feature across the superphylum. Like MK-D1, other Asgard archaea members of Lokiarchaeota, Helarchaeota, and Heimdallarchaeota may be capable of syntrophic AA degradation given that they encode an electron transfer complex FlxABCD-HdrABC associated with syntrophic bacteria²⁶ or formate dehydrogenases. Many lineages also possess genes for alternative electron disposal through fermentation – *i.e.*, reduction of pyruvate and acetyl-CoA to propionate and butyrate correspondingly (see Fig. 4b for details). Many lineages also encode the potential for other metabolisms – mono/tri-methylamine-driven homoacetogenesis and coupled H₂/S⁰ metabolism in Thorarchaeota; H₂S metabolism in Heimdallarchaeota; and, as pointed out by pioneering studies, Wood-Ljungdahl pathway in several genomes^{7,8,10,14}; alkane metabolism in Helarchaeota¹¹; and aerobic respiration in Heimdallarchaeota⁶. Although these metabolisms are highly unique and ecologically important, they are either only sporadically present or confined to specific phylum-level lineages. To identify potentially ancestral features, we searched for catabolic genes conserved across phylum-level lineages including Heimdallarchaeota (the most deep-branching Asgard archaea) that form monophyletic clusters in phylogenetic analyses. We found key catabolic genes for serine, threonine, and histidine degradation (serine/threonine dehydratase and urocanate hydratase; Supplementary Figs. S6 and S7), butyrate fermentation (3-ketoacyl-CoA thiolase and fatty-acid--CoA ligase; Supplementary Figs. S8 and S9), and propionate fermentation (succinate dehydrogenase flavoprotein subunit, methylmalonyl-CoA transcarboxylase-associated biotin ligase, and biotin carboxyl carrier protein; Supplementary Figs. S10–S12). Given the physiology of the isolated MK-D1, presence of AA catabolism, H₂ metabolism, and lack of biosynthetic pathways in nearly all extant Asgard archaea lineages, and conservation of the above metabolisms, we propose that the last Asgard archaea common ancestor was an AA-degrading anaerobe producing H₂ and fatty acids as byproducts that acquired ATP primarily from substrate-level phosphorylation from catabolizing 2-oxoacid intermediates and depended on metabolic partners, though we do not reject the possibility of other additional lifestyles.

231 **Proposal of new eukaryogenesis model**

232 We demonstrate that Asgard archaea are capable of syntrophic AA degradation and
233 identify related metabolic features conserved across the superphylum. This provides
234 tangible evidence for the recent proposal that the ancestral Asgard archaeon was a
235 syntrophic organotroph based on the prevalence of NiFe hydrogenases and
236 hydrogenogenic organotrophy across the superphylum¹⁴. In Earth's early ocean, partners
237 were likely methanogenic archaea rather than SRB due to low ocean sulfate
238 concentrations prior to the Great Oxidation Event (G.O.E.; 2.7 Ga~)²⁷ (Fig. 5a). As the
239 ocean and atmosphere became oxygenated, marine sulfate concentrations rose²⁸ and
240 syntropy likely shifted to interaction with SRB as observed in this study, which is more
241 thermodynamically favorable²⁹. During the G.O.E., cyanobacterial activity (and
242 concomitant marine organic matter production) increased, leading to transfer of excess
243 organic matter from the photic zone to marine sediments^{30,31}. The ancient anaerobic
244 Asgard archaea could have taken one of two paths for survival and adaptation: to remain
245 confined in strictly anaerobic habitats or to advance towards the anoxic-oxic interface
246 with greater substrate and “energy” availability. The archaeon at the last Archaea-
247 Eukarya division (*i.e.*, Heimdallarchaeota-Eukarya ancestor) likely preferentially grew
248 closer to the sulfate- and organics-rich anoxic-oxic interface environments (SRB could
249 have continued syntrophic interaction at the anoxic-oxic interface as many extant SRB
250 are aerotolerant and can perform sulfate reduction in the presence of O₂³²). However, to
251 further adapt to higher O₂ concentrations and also compete with facultatively aerobic
252 organotrophs, acquisition of the capacity for O₂ utilization would have been necessary.

253 Two routes may be possible: acquisition of aerobic respiration (*i.e.*, electron transport
254 chain and terminal oxidases) or an O₂-utilizing endosymbiont. We hypothesize that the
255 ancestral Heimdallarchaeon (or a specific sub-lineage) adopted the former route (Fig. 4b)
256 and the pre-last eukaryotic common ancestor (LECA) archaeon took the latter. Prior to
257 endosymbiosis, the pre-LECA archaeon likely interacted with SRB and O₂-utilizing
258 organotrophs, who maintained the local habitats O₂ concentrations low (Fig. 5b). The O₂-
259 utilizing partner was likely a facultative aerobe capable of aerobic and anaerobic H₂-
260 generating organotrophy. In this three-member interaction, the SRB could syntrophically
261 scavenge H₂ from both the pre-LECA archaeon and facultatively aerobic partner. The
262 dynamic oxic-anoxic-adaptable symbiosis could have strengthened the three-member
263 interaction and physical association. Moreover, the pre-LECA archaeon is predicted to

264 lack many biosynthetic pathways (Extended Data Fig. 4) and, thus, would have still
265 depended on metabolite exchange with partners for growth. One of the facultatively
266 aerobic partners was likely the pre-mitochondrial alphaproteobacterium (PA; *i.e.*, future
267 mitochondrion) as it has been proposed that PA would be capable of aerobic and
268 anaerobic H₂-generating organotrophy⁴. Evolution of the symbiosis likely led to PA
269 endosymbiosis into the pre-LECA archaeon, resulting in a transitional PA-containing pre-
270 LECA archaeon (PAPLA) using PA as an O₂-scavenging and building-block-providing
271 symbiont essential for growth under microaerobic conditions even without SRB.

272 Note that it is entirely possible for the H₂-consuming partner to have become
273 endosymbionts of the pre-LECA archaeon as proposed previously^{14,33}. However, H₂-
274 consuming partners would have had less advantage as endosymbionts. H₂ consumers
275 would prefer higher H₂ concentrations, but an enlarged host would require larger amounts
276 of substrate to accumulate H₂ compared to a small prokaryotic H₂ producers with
277 concentrated H₂ generation. Moreover, H₂ is membrane-permeable, so there is little
278 benefit to being inside an H₂ producer. Thus, endosymbiosis of an H₂ utilizer is
279 unfavorable without uncompartimentalized H₂ generation and unlikely to have stabilized.
280 In fact, extant methanogenic endosymbionts are observed only in hydrogenosome-
281 possessing protozoa³⁴.

282 How did the endosymbiosis physically manifest? Given the structure of extant
283 eukaryotic cells, it is logical to presume that the pre-LECA archaeon engulfed their
284 metabolic partner. Although a phagocytosis-like process has been previously proposed⁶,
285 (i) the observed MK-D1 cells are much too small to engulf their metabolic partner in this
286 way, (ii) Asgard archaea lack phagocytotic machinery³⁵, and (iii) a pre-mitochondriate
287 organism lacks sufficient energy to perform phagocytosis³⁶. Based on the observation of
288 unusual morphological structures of MK-D1 cells (Fig. 3 and Extended Data Fig. 2), the
289 pre-LECA Asgard archaeon may have produced protrusions and/or MVs (Fig. 5b). For
290 an archaeon syntrophically growing in a narrow space (*e.g.*, sediment pore), it may have
291 been possible for the protrusions/MVs to fuse and inadvertently surround its partner,
292 resulting in phagocytosis-independent engulfment (Fig. 5c). There are many possible
293 triggers for membrane fusion, including mechanical stress, electric current, or even
294 evolution of membrane-fusing proteins (*e.g.*, SNARE)³⁷. Unlike phagocytosis, such a
295 process would assimilate the partner and simultaneously form a chromosome-bounding

296 membrane structure topologically similar to that of the eukaryotic nuclear membrane (Fig.
297 5d), a scheme similar to the “Inside-out model” presented by Baum and Baum (2014)³⁸.

298 PAPLA likely shared 2-oxoacids with the endosymbiotic PA, given that AA-
299 degrading pathways widely encoded by Asgard archaea primarily recover ATP from 2-
300 oxoacid degradation (*i.e.*, 2-oxoacid oxidation and acyl-CoA hydrolysis; Figs. 4b and 5d).
301 Under anaerobic conditions, PAPLA and PA may have shared AA-derived 2-oxoacids
302 and both produced H₂ for syntrophic interaction with SRB. Conversely, when exposed to
303 microaerobic conditions, PAPLA likely catabolized AA in syntropy with SRB but also
304 provided 2-oxacids to PA and stimulate O₂ consumption. PAPLA could have
305 theoretically absorbed the endosymbiotic PA’s metabolic capacity to become a more
306 metabolically versatile unicellular organism; however, maintaining a respiratory
307 endosymbiont was likely beneficial because the high surface-area-to-volume ratio of
308 endosymbiotic (smaller) cells can maximize electron-driven energy synthesis (*i.e.*,
309 oxidative phosphorylation), which is kinetically limited by membrane surface area.
310 Moreover, the O₂-consuming symbiont could theoretically produce large amounts of
311 energy for biosynthesis and allow the host PAPLA access to an intracellular pool of
312 biological building blocks (*e.g.*, cofactors) without the need for active transport by
313 PAPLA itself.

314 To mature the endosymbiosis, streamlining of metabolic processes is paramount.
315 Two major redundancies are lipid biosynthesis and 2-oxoacid-driven ATP generation. As
316 the hosting PAPLA had ether-type lipids (as evidenced by MK-D1; Fig. 3j) and PA likely
317 had ester-type, two lipid types coexisted in the hybrid cell (Fig. 5d). As horizontal gene
318 transfer between the host and symbiont (or potentially other bacterial source) proceeded,
319 PAPLA likely lost synthesis of ether-type lipids and acquired that of ester-type to resolve
320 redundancy (*i.e.*, streamline genome) in lipid biosynthesis, and passively exchanged the
321 ether-type lipids with ester-type through dilution via cell division (lipid types can mix
322 without compromising structure/fluidity³⁹). Combining the engulfment described above
323 and this lipid exchange, we reach a PAPLA with single-layered ester-type lipid plasma
324 and nuclear membranes, which is consistent with extant eukaryotes (Fig. 5e).

325 Although PAPLA and PA initially shared 2-oxoacids, to streamline, this symbiosis
326 must transition towards delegation of this catabolism to one side and sharing of the
327 generated ATP. For maximizing aerobic oxidative phosphorylation, it is reasonable for
328 PA to catabolize 2-oxoacids, generate ATP, and transport ATP to the host cytosol. This

329 is analogous to the symbiosis between extant eukaryotes and their mitochondria (or
330 hydrogenosomes) and, thus, evolution of the ATP transporter (*i.e.*, ADP/ATP carrier or
331 AAC) was a major factor in fixing the symbiosis⁴⁰. However, it is unrealistic to think that
332 ATP-providing machinery evolved altruistically. We hypothesize that PA first developed
333 AAC as a parasitic tool to absorb host-synthesized ATP, as in extant pathogenic *Rickettsia*
334 and *Chlamydiae*⁴¹ (Fig. 5e). To combat this parasitism, PAPLA could have evolved to (i)
335 lose pyruvate (and other 2-oxoacids) catabolism, then (ii) delegate 2-oxoacid degradation
336 and ATP synthesis to PA, (iii) generate an ATP concentration gradient from PA to the
337 cytosol, and ultimately (iv) reverse the direction of AAC activity⁴¹ (Fig. 5f). For PAPLA
338 to evolve towards retaining both aerobic and anaerobic metabolism, the progression
339 above is critical because PAPLA-PA symbiosis would have heavily leaned towards
340 parasitism under anaerobic conditions (*i.e.*, taking both 2-oxoacids and ATP and ATP
341 with little to no return). On the other hand, adaptation to aerobic conditions through loss
342 of O₂-sensitive ferredoxin-dependent 2-oxoacid metabolism (*e.g.*, pyruvate:ferredoxin
343 oxidoreductase) and consequent delegation of 2-oxoacid-degrading ATP generation to
344 PA (via 2-oxoacid dehydrogenases) would have allowed evolution towards aerobiosis. In
345 this symbiosis, PAPLA and PA mutually benefit – PAPLA can allot energy metabolism
346 to PA and indirectly obtain energy from organotrophy via AAC while PA is fed 2-
347 oxoacids for energy production (Fig. 5f). Here, PAPLA enslaves PA and we arrive at
348 LECA possessing symbiosis congruent with that of extant eukaryotes and their
349 mitochondria.

350 In summary, we obtained the first isolate of Asgard archaea with unique metabolic
351 and morphological features through a total of 12 years cultivation, and combining these
352 observations with genomic analyses, propose the “Entangle-Engulf-Enslave (E³) model”
353 for eukaryogenesis from archaea. Maturation of this model requires elucidation and
354 incorporation of the timing/progression of lateral gene transfer between PAPLA and PA
355 or other bacteria, PA simplification and organellogenesis towards the first mitochondrion,
356 cell complexification (*e.g.*, non-mitochondrial organelle development), and elaboration
357 of eukaryotic cell division and their ties with Earth’s history. Endeavors in cultivation of
358 other Asgard archaea and more deep-branching eukaryotes are essential to further unveil
359 the road from archaea to eukaryotes.

360

361

362 **References**

- 363 1. Embley, T. M. & Martin, W. Eukaryotic evolution, changes and challenges. *Nature*
364 **440**, 623–630 (2006).
- 365 2. López-García, P. & Moreira, D. Open questions on the origin of eukaryotes.
Trends Ecol. Evol. **30**, 697-708 (2015).
- 366 3. Koonin, E. V. Origin of eukaryotes from within archaea, archaeal eukaryome and
368 bursts of gene gain: eukaryogenesis just made easier? *Phil. Trans. R. Soc. Lond. B*
369 **370**, 20140333 (2015).
- 370 4. Martin, W. F., Garg, S. & Zimorski, V. Endosymbiotic theories for eukaryote
371 origin. *Phil. Trans. R. Soc. Lond. B* **370**, 20140330 (2015).
- 372 5. Spang, A. *et al.* Complex archaea that bridge the gap between prokaryotes and
373 eukaryotes. *Nature* **521**, 173–179 (2015).
- 374 6. Zaremba-Niedzwiedzka, K. *et al.* Asgard archaea illuminate the origin of
375 eukaryotic cellular complexity. *Nature* **541**, 353–358 (2017).
- 376 7. Sousa, F. L., Neukirchen, S., Allen, J. F., Lane, N. & Martin, W. F. Lokiarchaeon
377 is hydrogen dependent. *Nat. Microbiol.* **1**, 16034 (2016).
- 378 8. Seitz, K. W., Lazar, C. S., Hinrichs, K.-U., Teske, A. P. & Baker, B. J. Genomic
379 reconstruction of a novel, deeply branched sediment archaeal phylum with
380 pathways for acetogenesis and sulfur reduction. *ISME J.* **10**, 1696–1705 (2016).
- 381 9. Dombrowski, N., Teske, A. P. & Baker, B. J. Expansive microbial metabolic
382 versatility and biodiversity in dynamic Guaymas Basin hydrothermal sediments.
Nat. Commun. **9**, 4999 (2018).
- 384 10. Liu, Y. *et al.* Comparative genomic inference suggests mixotrophic lifestyle for
385 Thorarchaeota. *ISME J.* **12**, 1021–1031 (2018).
- 386 11. Seitz, K. W. *et al.* Asgard archaea capable of anaerobic hydrocarbon cycling. *Nat.*
387 *Commun.* **10**, 1822 (2019).
- 388 12. Pushkarev, A. *et al.* A distinct abundant group of microbial rhodopsins discovered
389 using functional metagenomics. *Nature* **558**, 595–599 (2018).
- 390 13. Bulzu, P.-A. *et al.* Casting light on Asgardarchaeota metabolism in a sunlit
391 microoxic niche. *Nat. Microbiol.* **105**, 20356 (2019).
- 392 14. Spang, A. *et al.* Proposal of the reverse flow model for the origin of the eukaryotic
393 cell based on comparative analyses of Asgard archaeal metabolism. *Nat. Microbiol.*
394 **4**, 1138–1148 (2019).

- 395 15. Aoki, M. *et al.* A long-term cultivation of an anaerobic methane-oxidizing
396 microbial community from deep-sea methane-seep sediment using a continuous-
397 flow bioreactor. *PLoS ONE* **9**, e105356 (2014).
- 398 16. Schink, B. & Stams, A. J. *Syntrophism Among Prokaryotes in The Prokaryotes*
399 (eds. Rosenberg, E., DeLong, E. F., Lory, S., Stackebrandt, E. & Thompson, F.)
400 471–493 (Springer Berlin Heidelberg, 2013).
- 401 17. Knittel, K., Lösekann, T., Boetius, A., Kort, R. & Amann, R. Diversity and
402 distribution of methanotrophic archaea at cold seeps. *Appl. Environ. Microbiol.* **71**,
403 467–479 (2005).
- 404 18. Marguet, E. *et al.* Membrane vesicles, nanopods and/or nanotubes produced by
405 hyperthermophilic archaea of the genus *Thermococcus*. *Biochem. Soc. Trans.* **41**,
406 436–442 (2013).
- 407 19. Imachi, H. *et al.* Cultivation of methanogenic community from subseafloor
408 sediments using a continuous-flow bioreactor. *ISME J.* **5**, 1913–1925 (2011).
- 409 20. Da Cunha, V., Gaia, M., Gadelle, D., Nasir, A. & Forterre, P. Lokiarchaea are close
410 relatives of Euryarchaeota, not bridging the gap between prokaryotes and
411 eukaryotes. *PLoS Genet.* **13**, e1006810 (2017).
- 412 21. Da Cunha, V., Gaia, M., Nasir, A. & Forterre, P. Asgard archaea do not close the
413 debate about the universal tree of life topology. *PLoS Genet.* **14**, e1007215 (2018).
- 414 22. Spang, A. *et al.* Asgard archaea are the closest prokaryotic relatives of eukaryotes.
415 *PLoS Genet.* **14**, e1007080 (2018).
- 416 23. Brunk, C. F. & Martin, W. F. Archaeal histone contributions to the origin of
417 eukaryotes. *Trends Microbiol.* **27**, 703–714 (2019).
- 418 24. Buckel, W. & Thauer, R. K. Energy conservation via electron bifurcating
419 ferredoxin reduction and proton/ Na^+ translocating ferredoxin oxidation. *Biochim.
420 Biophys. Acta* **1827**, 94–113 (2013).
- 421 25. Ma, K., Zhou, H. Z. & Adams, M. W. Hydrogen production from pyruvate by
422 enzymes purified from the hyperthermophilic archaeon, *Pyrococcus furiosus*: A
423 key role for NADPH. *FEMS Microbiol. Lett.* **122**, 245–250 (1994).
- 424 26. Nobu, M. K. *et al.* The genome of *Syntrophorhabdus aromaticivorans* strain UI
425 provides new insights for syntrophic aromatic compound metabolism and electron
426 flow. *Environ. Microbiol.* **17**, 4861–4872 (2015).
- 427 27. Canfield, D. E., Habicht, K. S. & Thamdrup, B. The Archean sulfur cycle and the

- early history of atmospheric oxygen. *Science* **288**, 658–661 (2000).

28. Luo, G. *et al.* Rapid oxygenation of Earth’s atmosphere 2.33 billion years ago. *Sci. Adv.* **2**, e1600134 (2016).

29. Valentine, D. L. *Thermodynamic Ecology of Hydrogen-based Syntrophy in Symbiosis. Cellular Origin, Life in Extreme Habitats and Astrobiology*, (ed. Seckbach, J.) **4**, 147–161 (Springer, Dordrecht, 2001).

30. Kump, L. R. *et al.* Isotopic evidence for massive oxidation of organic matter following the Great Oxidation Event. *Science* **334**, 1694–1696 (2011).

31. Gumsley, A. P. *et al.* Timing and tempo of the Great Oxidation Event. *Proc. Natl. Acad. Sci. USA* **114**, 1811–1816 (2017).

32. Cypionka, H. Oxygen respiration by *Desulfovibrio* species. *Annu. Rev. Microbiol.* **54**, 827–848 (2000).

33. López-García, P. & Moreira, D. Selective forces for the origin of the eukaryotic nucleus. *BioEssays* **28**, 525–533 (2006).

34. *(Endo)symbiotic Methanogenic Archaea*. (ed. Hackstein, J. H. P.) (Springer, 2018).

35. Burns, J. A., Pittis, A. A. & Kim, E. Gene-based predictive models of trophic modes suggest Asgard archaea are not phagocytotic. *Nat. Ecol. Evol.* **2**, 697–704 (2018).

36. Martin, W. F., Tielens, A. G. M., Mentel, M., Garg, S. G. & Gould, S. B. The physiology of phagocytosis in the context of mitochondrial origin. *Microbiol. Mol. Biol. Rev.* **81**, e00008–17 (2017).

37. Cevc, G. & Richardsen, H. Lipid vesicles and membrane fusion. *Adv. Drug Deliv. Rev.* **38**, 207–232 (1999).

38. Baum, D. A. & Baum, B. An inside-out origin for the eukaryotic cell. *BMC Biol.* **12**, 76 (2014).

39. Batenjany, M. M., O’Leary, T. J., Levin, I. W. & Mason, J. T. Packing characteristics of two-component bilayers composed of ester- and ether-linked phospholipids. *Biophys. J.* **72**, 1695–1700 (1997).

40. Gray, M. W. The pre-endosymbiont hypothesis: a new perspective on the origin and evolution of mitochondria. *Cold Spring Harb. Perspect. Biol.* **6**, a016097 (2014).

41. Winkler, H. H. & Neuhaus, H. E. Non-mitochondrial ATP transport. *Trends Biochem. Sci.* **24**, 64–68 (1999).

461 **Supplementary Information** is available in the online version of the paper.

462

463 **Acknowledgements** We thank Hiroyuki Ohno and Tsuyoshi Yamaguchi for assistance
464 with HCR-FISH analysis, Takeshi Terada for help of NanoSIMS sample preparation,
465 Masami Isozaki for assistance with cultivation experiments, Takaaki Kubota for
466 assistance with chemical analysis, Kiyotaka Takishita, Akinori Yabuki, Takashi Shiratori,
467 Akiyoshi Ohashi, Fumio Inagaki, Takuro Nunora, Shinsuke Kawagucci, Takazo Shibuya,
468 Shun'ichi Ishii, Yusuke Tsukatani and Yutetsu Kuruma for useful advice and discussion
469 and Ai Miyashita, Yuto Yashiro, Ken Aoi, Masayuki Ehara, Masataka Aoki and Yayoi
470 Saito for assistance with the bioreactor operation. We also thank Juichiro Ashi and the
471 R/V Yokosuka and “*Shinkai 6500*” operation team during cruise YK06-03 (JAMSTEC)
472 and the shipboard scientists and crews of the *Chikyu* Shakedown Cruise CK06-06 for
473 their assistance in collecting samples. This study was partially supported by grants from
474 the Japan Society for the Promotion of Science (JSPS) (KAKENHI Grants 18687006,
475 21687006, 24687011, 15H02419 and 19H01005 to H.I., 18H03367 to M.K.N., 26710012,
476 18H02426, 18H05295 to H.T., and Grant-in-Aid for JSPS Fellow 16J10845 to N.N.).
477 This work was also supported by JSPS KAKENHI Grant Number JP16H06280, Grant-
478 in-Aid for Scientific Research on Innovative Areas – Platforms for Advanced
479 Technologies and Research Resources “Advanced Bioimaging Support” and the
480 Cooperative Study Program (19-504) of National Institute for Physiological Sciences.
481

482

483 **Author contributions** H.I. conceived the study and deep marine sediment sampling. H.I.,
484 N.N., M.O., M.M. and S.S. conducted cultivation and culture-based experiments. M.K.N.
485 and Y.Takaki performed genome analysis. H.I., N.N., Y.Morono, M.O., T.I., M.I., K.M.,
486 C.S. and K.U. undertook the microscopy and NanoSIMS work. M.O., Y.S. and Y.Y.
487 performed qPCR, SSU rRNA gene analysis and DNA/RNA sequencing. Y.Takano, Y.
488 Matsui and E.T. performed chemical analysis. H.I., M.K.N., N.N., Y.Morono, Y. Takaki,
489 Y.Takano, K.M., C.S., T.Y. Y.K. H.T. and K.T. conducted data interpretation. H.I.,
490 M.K.N., Y.Takano, H.T., Y.K. and K.T. wrote the manuscript with input from all co-
authors. All authors have read and approved the manuscript submission.

491

492 **Author Information** The authors declare no competing financial interests.
493 Correspondence and requests for materials should be addressed to H.I
494 (imachi@jamstec.go.jp) or M.K.N. (m.nobu@aist.go.jp).
495

496 **Methods**

497 No statistical methods were used to predetermine sample size.

498 **Sampling site and sample description.** A 25-cm long sediment core (949C3) was
499 collected from a methane-seep site at the Omine Ridge, Nankai Trough, off the Kumano
500 area, Japan (33°7.2253'N, 136°28.6672'E), 2,533 m below the sea level, via the manned
501 submersible “*Shinkai 6500*” (cruise YK06-03, dive no. 6K949, May 6th, 2006). The
502 detailed sediment core sample and site information has been described previously^{15,42,43}.
503 Our previous geochemical and 16S rRNA gene analysis indicated that the occurrence of
504 anaerobic oxidation of methane (AOM) reactions mediated by archaeal anaerobic
505 methanotrophs (ANMEs) in the sediment^{15,42}. The SSU rRNA gene analysis also showed
506 that the sediment contained abundant and diverse microorganisms, most of which were
507 affiliated with uncultured microbial groups, including Asgard archaea^{15,42}.

508 **Culturing.** The deep-sea methane-seep sediment sample was first enriched using a
509 continuous-flow bioreactor system supplemented with methane as the major energy
510 source. The bioreactor, called a down-flow hanging sponge (DHS) bioreactor, has
511 operated in our laboratory, JAMSTEC, Yokosuka Headquarters, since December 28,
512 2006. The detailed operation conditions for the DHS bioreactor have been described
513 previously¹⁵. To isolate anaerobic microorganisms, including Asgard archaea, from the
514 DHS reactor, 2 ml samples of the bioreactor enrichment sediment slurry were inoculated
515 in 15 ml glass tubes with a simple substrate and a basal medium. The composition of the
516 basal medium was almost similar to that used for cultivation in the DHS bioreactor¹⁵, but
517 it did not contain sulfate (i.e., Na₂SO₄). The basal medium composition was as follows
518 (per liter): 9.47 g MgCl₂·6H₂O, 1.36 g CaCl₂·2H₂O, 20.7 g NaCl, 0.54 g NH₄Cl, 0.14 g
519 KH₂PO₄, 2.7 g NaHCO₃, 0.3 g Na₂S·9H₂O, 0.3 g cysteine·HCl, 1 ml trace element
520 solution¹⁵, 1 ml Se/W solution, 2 ml vitamin solution¹⁵ and resazurin solution (1 mg/ml).
521 The medium was purged with N₂/CO₂ gas (80:20, v/v), and the pH was adjusted to 7.5 at
522 25°C. The culture tubes were sealed with butyl rubber stoppers and screw caps.
523 Autoclaved or filter-sterilized organic substances (such as protein-derived materials,
524 sugars, and fatty acids) were added to the tubes with stock solutions prior to inoculation

525 with the bioreactor enriched community. After establishing a stable *Ca. P. syntrophicum*
526 culture, cultivations were performed at 20°C in 50-ml serum vials containing 20 ml basal
527 medium supplemented with CA (0.05%, w/v), 20 AAs (0.1 mM each), and PM (0.1%,
528 w/v, Hohoemi, Meiji Co., Ltd.) under an atmosphere of N₂/CO₂ (80:20, v/v) in the dark
529 without shaking, unless mentioned otherwise. Information regarding the purity check of
530 MK-D1 cultures, as well as additional information about cultivation, is described in the
531 Supplementary Methods.

532 **SSU rRNA gene-based analysis.** DNA extraction and PCR mixture preparation were
533 performed on a clean bench to reduce contamination. DNA extraction from culture
534 samples was performed as described previously⁴⁴. The concentration of extracted DNA
535 was measured using a Quant-iT dsDNA High-Sensitivity Assay Kit (Life Technologies).
536 PCR amplification was performed using the TaKaRa Ex *Taq* (for conventional clone
537 analysis) or TaKaRa LA *Taq* (for Illumina-based amplicon sequencing [iTAG] for
538 targeted sequencing for the SSU rRNA gene analysis) (TaKaRa Bio Inc.), and the reaction
539 mixtures for PCR were prepared according to the manufacturer's instructions. For the
540 conventional clone analysis, a universal primer pair 530F/907R⁴² and an archaeal primer
541 pair 340F/932R^{15,45} were used for PCR amplification. For iTAG analysis, the universal
542 primer pair 530F/907R, which contained overhang adapters at 5' ends, was used. The
543 procedures used for library construction, sequencing, and data analysis were described
544 previously^{19,46}.

545 **Growth monitoring using qPCR.** For the quantitative analysis, a StepOnePlus Real-
546 Time PCR System (Thermo Fisher Scientific) with a SYBR Premix Ex *Taq* II kit
547 (TaKaRa Bio Inc.) was used. The candidate phylum Lokiarchaeota-specific primer pair
548 MBGB525F/Ar912r was used for amplification of 16S rRNA genes. Primer MBGB525F
549 is the complementary sequence of the MGBG525 probe¹⁷, while Ar912r is an archaeal
550 universal primer that is a slightly modified version of the original designed primer⁴⁷. The
551 detailed procedure for qPCR is described in the Supplementary Methods. The doubling
552 times of MK-D1 were calculated based on the semilogarithmic plot of the qPCR data.

553 **Growth test with multiple substrates.** To examine effect of the presence of other
554 substances on growth of MK-D1, CA-20 AAs-PM medium supplemented with an
555 individual substrate (Extended Data Table 3) was prepared, followed by qPCR and iTAG
556 analyses. Each cultivation condition was set in duplicate; however, the H₂-fed culture was
557 prepared in triplicate because Sousa *et al.* (2016)⁷ reported that a *Lokiarchaeum* has

558 potential to grow with hydrogen based on a comparative genome analysis. Detailed
559 culture liquid sampling and the subsequent qPCR and iTAG analyses are described in the
560 Supplementary Materials.

561 **Evaluation of growth temperature.** The test was performed using a basal medium
562 containing CA and PM, with a pure co-culture of MK-D1 and *Methanogenium* as the
563 inoculum (20%, v/v). The cultures were incubated at 4, 10, 15, 20, 25, 30, 37, and 40°C.
564 All incubations for the test were performed in triplicate. After 100 days of incubation,
565 16S rRNA gene copy numbers of MK-D1 were evaluated through qPCR technique.

566 **FISH.** Fixation of microbial cells, storage of the fixed cells, and standard FISH were
567 performed in accordance with a previously described protocol¹⁹. The 16S rRNA-targeted
568 oligonucleotide probes used in this study are listed in Supplementary Table S3. The
569 designing of MK-D1-specific probes is described in the Supplementary Methods. As
570 clear fluorescent signals were not obtained using the standard FISH technique, we
571 employed an *in situ* DNA-hybridization chain reaction (HCR) technique⁴⁸. The FISH
572 samples were observed using epifluorescence microscopes (BX51 or BX53, Olympus)
573 and a confocal laser scanning microscope (Nikon A1RMP, Nikon Instech).

574 **SEM.** Microbial cells were fixed overnight in 2.5% (w/v) glutaraldehyde in the CA-20
575 AAs medium at 20°C. The sample preparation procedure has been described previously⁴⁹.
576 The cell samples were observed under a field emission (FE)-SEM (JSM-6700F, JEOL)
577 or an extreme high-resolution FIB-SEM (Helios G4 UX, ThermoFisher Scientific).

578 **Ultrathin sectioning and TEM.** Cells were prefixed with 2.5% (w/v) glutaraldehyde for
579 2 h. The specimens were frozen in a high-pressure freezing apparatus (EM-PACT2,
580 Leica)⁵⁰. The frozen samples were substituted with 2% OsO₄ in acetone for 3–4 days at -
581 80°C, and the samples were warmed gradually to room temperature, rinsed with acetone
582 embedded in epoxy resin (TAAB). Thin sections (70 nm) were cut with a ultramicrotome
583 (EM-UC7, Leica). Ultra-thin sections of the cells were stained with 2% uranyl acetate
584 and lead-stained solution (0.3% lead nitrate and 0.3% lead acetate, Sigma-Aldrich), and
585 were observed by a transmission electron microscopy (Tecnai 20, FEI) at an acceleration
586 voltage of 120 kV.

587 **Cryo-EM.** Due to the low cell yield-culture, 400 ml of the culture of MK-D1 was
588 prepared and concentrated to about 5 ml using a 0.22 µm-pore-size polyethersulfone
589 (PES) filter unit (Corning) in an anaerobic chamber (95:5 [v/v] N₂:H₂ atmosphere; COY
590 Laboratory Products). The concentrated culture liquid was placed in a glass vial in the

591 anaerobic chamber. After that, the head space of the glass vial was replaced by N₂/CO₂
592 gas (80:20, v/v). Immediately before the electron microscopic observation, the glass vial
593 was opened, and the liquid culture was concentrated to about 200 µl by centrifugation at
594 20,400 g for 10 min at 20°C. Subsequently, 3 µl of the concentrated liquid culture was
595 applied onto a Quantifoil Mo grid R1.2/1.3 (Quantifoil MicroTools) pretreated with glow-
596 discharge, and was plunged-frozen in liquid ethane using a Vitrobot Mark IV (FEI
597 Company) at 4°C and 95% humidity.

598 The frozen grid was mounted onto a 914 liquid-nitrogen cryo-specimen holder
599 (Gatan Inc.) and loaded into a JEM2200FS electron microscope (JEOL) equipped with a
600 field emission electron source operating at 200 kV and an omega-type in-column energy
601 filter (slit width: 20 eV). The images were recorded on a DE-20 direct detector camera
602 (Direct Electron LP.) at a nominal magnification of 15,000 x, which resulted in an
603 imaging resolution of 3.66 Å per pixel, with the total dose under 20 electrons per Å² using
604 a low dose system. For electron tomography, tilt series images were collected manually
605 in a range of ~± 62° at 2° increments. The total electron dose on the specimen per tilt
606 series was kept under 100 electrons per Å² to minimize radiation damage. The tilt series
607 were aligned using gold fiducials, and tomograms were reconstructed using filtered back
608 projection or SIRT in the IMOD software⁵¹ with an image binning of 5.

609 **Lipid analysis.** About 120 ml of a highly purified culture sample were concentrated using
610 the same method described above, except that the filtration concentration procedure was
611 performed on a clean bench instead of the anaerobic chamber. Following cell collection,
612 the cells were washed with the anaerobic basal medium to eliminate the interfering matrix.
613 Subsequently, lipid analysis was conducted for the collected cells after the improved
614 method⁵². For precise qualitative liquid analysis, gas chromatography (GC) combined
615 with mass spectrometry (MS) on the 7890 system (Agilent Technologies Inc.) was
616 conducted to compare the retention time and mass fragmentation signatures.

617 **Stable isotope probing and NanoSIMS analysis.** To confirm utilization of amino acids
618 by MK-D1, a stable isotope probing experiment was performed using a ¹³C- and ¹⁵N-
619 labeled amino acids mixture (Cambridge Isotope Laboratories). Briefly, 120 ml serum
620 vials containing 40 ml basal medium were prepared and supplemented with the stable
621 isotope labeled 20 AAs (roughly 0.1 mM of each), CA (0.05%, w/v) and non-labeled 20
622 AAs mixture (0.1 mM of each). Two types of highly purified cultures of MK-D1 were
623 used as inocula: a co-culture with *Methanobacterium* sp. strain MO-MB1 and a tri-culture

624 with *Halodesulfovibrio* and *Methanogenium*. The vials were incubated at 20°C in the dark
625 without shaking for 120 days. A reference cultivation was also performed under the same
626 cultivation condition without the addition of the stable isotope labeled 20 AAs mixture
627 (Extended Data Table 2). The detailed sample preparation and analysis method using
628 NanoSIMS is described in the Supplementary Methods.

629 **Chemical analysis.** The stable carbon isotope compositions of methane and carbon
630 dioxide in the sampled gas phase were analyzed as described previously (Okumura et al.
631 2016). Methane concentrations were measured by gas chromatography (GC-4000, GL
632 Science Inc., Tokyo, Japan) using a Shincarbon ST 50/80 column (1.0 m x 3.0 mm ID,
633 Shinwa Chem. Ind.) and a flame ionization detector with nitrogen as a carrier gas.

634 Amino acid concentrations in pure co-cultures of MK-D1 and *Methanogenium* were
635 quantified through a previously described method^{53,54}. In brief, we processed the acid
636 hydrolysis with 6 M HCl (110°C, 12 h) for the culture liquid samples after filtration using
637 a 0.2 µm pore-size polytetrafluoroethylene filter unit (Millipore). The amino acid fraction
638 was derivatized to N-pivaloyl iso-propyl esters prior to GC using a 6890N GC instrument
639 connected to the nitrogen phosphorus and flame ionization detectors (Agilent
640 Technologies Inc.). For cross-validation of qualitative identification of amino acids, GC-
641 MS on the 7890 system (Agilent Technologies Inc.) was used⁵².

642 **Genome sequencing and assembly.** DNA extraction was performed as described
643 previously⁴⁴. Mate-paired library with an average insert size of 3000 bp was constructed
644 according to the manufacturer's instructions with Nextera Mate Pair Library Preparation
645 kit (Illumina). Library sequencing was performed using Illumina MiSeq platform (2 x
646 300 bp), which resulted in 3,822,290 paired reads. The mate pair reads were processed as
647 follows: adapters and low-quality sequences were removed using Trimmomatic ver.
648 0.33⁵⁵, and the linker sequences were removed using NextClip ver. 1.3.1⁵⁶. *De novo*
649 assembly was performed using SPAdes ver 3.1.1⁵⁷ with multiple k-mer sizes (21, 33, 55,
650 77, and 99), which resulted in 3,487 contigs with lengths >500 bp, totaling upto 14.68
651 Mbp. The software MyCC⁵⁸ was used with default parameters for binning based on
652 genomic signatures, marker genes, and contig coverages. As heterogeneity in the
653 sequence can cause highly fragmented or redundant contigs, the ambiguous contigs
654 (sequence coverage < 5 or a length < 1kb) and redundant contigs were discarded from
655 binning. This resulted in the recovery of genomes related to Lokiarchaeum (i.e., *Ca. P.*
656 *syntrophicum* MK-D1, 4.46 Mbp), *Halodesulfovibrio* (4.13 Mbp) and *Methanogenium*

657 (2.33 Mbp). Scaffold for each bin were constructed using SSPACE ver. 3.0⁵⁹ with mate-
658 paired information of Illumina reads. To obtain the complete genome sequence of *Ca. P.*
659 *syntrophicum*, the gaps were filled using Sanger sequencing method. Genomes were
660 annotated using Prokka v1.12⁶⁰ and manually curated. The curation involved functional
661 domain analysis through CD-Search with its corresponding conserved domain
662 database^{61,62}; signal peptide and transmembrane domain prediction through SignalP
663 v4.1⁶³; carbohydrate-active enzyme, peptidase, and lipase prediction through dbCAN
664 5.0⁶⁴, MEROPS⁶⁵, and lipase engineering database⁶⁶; and hydrogenase annotation with
665 assistance from HydDB⁶⁷. In addition, to further verify the function, we compared the
666 sequence similarity of each gene to UNIPROTKB/SWISSPROT containing enzymes
667 with experimentally verified catalytic activity and genes with extensive genetic,
668 phylogenetic, and/or genomic characterizations^{68,69} with a 40% amino acid similarity
669 cutoff. For enzymes that have divergent functions even with a 40% similarity cutoff (e.g.,
670 [FeFe] and [NiFe] hydrogenases, 3-oxoacid oxidoreductases, glutamate dehydrogenases,
671 and sugar kinases), phylogenetic trees were constructed with reference sequences to
672 identify association of the query sequences to phylogenetic clusters containing enzymes
673 with characterized catalytic activity.

674 **Phylogenetic analysis.** Phylogenomic tree of MK-D1 and select cultured archaea,
675 eukaryotes, and bacteria. 31 ribosomal proteins conserved across the three domains
676 (Supplementary Table S4) were collected from MK-D1, the organisms shown in the tree,
677 and metagenome-assembled genomes (MAGs) of uncultured archaeal lineages
678 (Supplementary Table S5). Two alignments were performed in parallel: (i) only including
679 sequences from cultured organisms and (ii) also including MAG-derived sequences.
680 MAFFT v7 (--linsi) was used for alignment in both cases⁷⁰. For the latter, MAG-derived
681 sequences were included to generate an alignment that maximizes the archaeal diversity
682 taken into account, but removed for subsequent tree construction to avoid any influence
683 of contamination (*i.e.*, concatenation of sequences that do not belong to the same
684 organism). *Ca. Korarchaeum* sequences were kept in the tree based on the
685 cultured+uncultured alignment due to its critical phylogenetic position in TACK
686 phylogeny. After removing all-gap positions and concatenation, the maximum likelihood
687 trees were constructed using RAxML-NG (fixed empirical substitution matrix [LG], 4
688 discrete GAMMA categories, empirical AA frequencies, and 100 bootstrap replicates)⁷¹.
689 Bootstrap values around critical branching points are also shown. For 16S ribosomal

690 RNA phylogeny, sequences were aligned using SINA⁷² against the Silva v132
691 alignment⁷³. The maximum likelihood tree was calculated using RAxML⁷⁴ using fixed
692 empirical substitution matrix (LG), 4 discrete GAMMA categories, empirical amino acid
693 frequencies from the alignment, and 100 bootstrap replicates. For analysis of urocanate
694 hydratase, serine/threonine dehydratase, succinate dehydrogenase flavoprotein, fatty-
695 acid--CoA ligase, and 3-ketoacyl-CoA thiolase homologs were collected through
696 BLASTp analysis of the Asgard archaea sequences against the UniProt database (release
697 2019_06). Of homologs with sequence similarity $\geq 40\%$ and overlap $\geq 70\%$, representative
698 sequences were selected using CD-HIT with a clustering cutoff of 70% similarity (default
699 settings otherwise). Additional homologs with verified biochemical activity, sequence
700 similarity $\geq 30\%$, and overlap $\geq 70\%$ were collected through BLASTp analysis of the
701 Asgard archaea sequences against the UniProt/SwissProt database. Sequences were
702 aligned using MAFFT v7⁷⁰ with default settings and trimmed using trimAl⁷⁵ with default
703 settings. The phylogenetic tree was constructed using RAxML-NG⁷¹ using fixed
704 empirical substitution matrix (LG), 4 discrete GAMMA categories, empirical amino acid
705 frequencies from the alignment, and 100 bootstrap replicates.

706 For analysis of biotin ligase and biotin carboxyl carrier protein, homologs were
707 collected through BLASTp analysis of the Asgard archaea sequences against the UniProt
708 database (release 2019_06). Of homologs with sequence similarity $\geq 40\%$ and overlap
709 $\geq 70\%$, representative sequences were selected using CD-HIT with a clustering cutoff of
710 70% similarity (default settings otherwise). Additional homologs with verified
711 biochemical activity, sequence similarity $\geq 30\%$, and overlap $\geq 70\%$ were collected
712 through BLASTp analysis of the Asgard archaea sequences against the
713 UniProt/SwissProt database. Sequences were aligned using MAFFT v7⁷⁰ with default
714 settings and trimmed using trimAl⁷⁵ with default settings. The phylogenetic tree was
715 constructed using FastTree⁷⁶ using fixed empirical substitution matrix (LG) and 1000
716 bootstrap replicates.

717 **RNA based sequencing analysis.** To perform RNA based sequencing analysis, 100 ml
718 of culture liquid were prepared from five highly purified cultures that were incubated
719 with CA, 20 AAs, and PM for about 100 days at 20°C. Before RNA extraction, the growth
720 of MK-D1 was confirmed using the qPCR technique, and the cells density levels were
721 $\sim 10^5$ copies/ml in each culture.

722 To harvest microbial cells, the culture liquid was filtered through a 0.22- μm pore-
723 size mixed cellulose ester membrane filter (GSPW01300, Merck Millipore) on a clean
724 bench. After filtration, the membrane was cut in half with a sterilized scissors and then
725 directly inserted into the PowerBiofilm bead tubes of a PowerBiofilm RNA Isolation kit
726 (MO BIO Laboratories). The following RNA extraction procedures were performed
727 according to the manufacturer's instructions. The extracted RNA was applied to an RNA
728 clean & concentrator kit-5 (Zymo Research) for concentration. The obtained RNA was
729 quantified using an Agilent 2100 Bioanalyzer system with an RNA Pico kit (Agilent
730 Technologies) and then applied to an Ovation Universal RNA-Seq System (NuGEN
731 Technologies) for the construction of an RNA sequence library. At the step for Insert
732 Dependent Adaptor Cleavage technology mediated adaptor cleavage during the library
733 construction, specific primers for 16S rRNA and 23S rRNA genes of MK-D1 were used
734 to reduce rRNA gene sequences from the cDNA pool. The constructed cDNA library was
735 sequenced using the MiSeq platform (Illumina).

736 The raw RNA sequencing data were trimmed by removal of the adapters and low-
737 quality sequences using Trimmomatic ver. 0.33⁵⁵. The expression abundance of all coding
738 transcripts was estimated in RPKM values using EDGE-pro ver. 1.3.1⁷⁷.

739 **Data availability.** Genomes for *Ca. Prometheoarchaeum syntrophicum* MK-D1,
740 *Halodesulfobacter* sp. MK-HDV, and *Methanogenium* sp. MK-MG are available under
741 Genbank BioProjects PRJNA557562, PRJNA557563, and PRJNA557565 respectively.
742 The iTAG sequence data was deposited in Bioproject PRJDB8518 with the accession
743 numbers DRR184081–DRR184101. The 16S rRNA gene sequences of MK-D1,
744 *Halodesulfobacter* sp. MK-HDV, *Methanogenium* sp. MK-MG and clones obtained from
745 primary enrichment culture were deposited in the DDBJ/EMBL/GenBank database under
746 accession numbers LC490619–LC490624.

747

- 748 42. Nunoura, T. *et al.* Microbial diversity in deep-sea methane seep sediments
749 presented by SSU rRNA gene tag sequencing. *Microbes Environ.* **27**, 382–
750 390 (2012).
- 751 43. Toki, T., Higa, R., Ijiri, A., Tsunogai, U. & Ashi, J. Origin and transport of
752 pore fluids in the Nankai accretionary prism inferred from chemical and
753 isotopic compositions of pore water at cold seep sites off Kumano. *Earth
754 Planet Space* **66**, 137 (2014).

- 755 44. Nakahara, N. *et al.* *Aggregatilinea lenta* gen. nov., sp. nov., a slow-growing,
756 facultatively anaerobic bacterium isolated from subseafloor sediment, and
757 proposal of the new order *Aggregatilineales* ord. nov. within the class
758 *Anaerolineae* of the phylum *Chloroflexi*. *Int. J. Syst. Evol. Microbiol.* **69**,
759 1185–1194 (2019).
- 760 45. Murakami, S., Fujishima, K., Tomita, M. & Kanai, A. Metatranscriptomic
761 analysis of microbes in an oceanfront deep-subsurface hot spring reveals
762 novel small RNAs and type-specific tRNA degradation. *Appl. Environ.*
763 *Microbiol.* **78**, 1015–1022 (2012).
- 764 46. Imachi, H. *et al.* Cultivable microbial community in 2-km-deep, 20-million-
765 year-old subseafloor coalbeds through ~1000 days anaerobic bioreactor
766 cultivation. *Sci. Rep.* **9**, 2305 (2019).
- 767 47. Miyashita, A. *et al.* Development of 16S rRNA gene-targeted primers for
768 detection of archaeal anaerobic methanotrophs (ANMEs). *FEMS Microbiol.*
769 *Lett.* **297**, 31–37 (2009).
- 770 48. Yamaguchi, T. *et al.* In situ DNA-hybridization chain reaction (HCR): a
771 facilitated in situ HCR system for the detection of environmental
772 microorganisms. *Environ. Microbiol.* **17**, 2532–2541 (2015).
- 773 49. Miyazaki, M. *et al.* *Sphaerochaeta multiformis* sp. nov., an anaerobic,
774 psychrophilic bacterium isolated from subseafloor sediment, and emended
775 description of the genus *Sphaerochaeta*. *Int. J. Syst. Evol. Microbiol.* **64**,
776 4147–4154 (2014).
- 777 50. Toyooka, K. *et al.* Wide-range high-resolution transmission electron
778 microscopy reveals morphological and distributional changes of
779 endomembrane compartments during log to stationary transition of growth
780 phase in tobacco BY-2 cells. *Plant Cell Physiol.* **55**, 1544–1555 (2014).
- 781 51. Kremer, J. R., Mastronarde, D. N. & McIntosh, J. R. Computer visualization
782 of three-dimensional image data using IMOD. *J. Struct. Biol.* **116**, 71–76
783 (1996).
- 784 52. Takano, Y. *et al.* Insight into anaerobic methanotrophy from $^{13}\text{C}/^{12}\text{C}$ -amino
785 acids and $^{14}\text{C}/^{12}\text{C}$ -ANME cells in seafloor microbial ecology. *Sci. Rep.* **8**,
786 14070 (2018).
- 787 53. Takano, Y., Kashiyama, Y., Ogawa, N. O., Chikaraishi, Y. & Ohkouchi, N.

- 788 Isolation and desalting with cation-exchange chromatography for
789 compound-specific nitrogen isotope analysis of amino acids: application to
790 biogeochemical samples. *Rapid Commun. Mass Spectrom.* **24**, 2317–2323
791 (2010).
- 792 54. Chikaraishi, Y. *et al.* *Instrumental Optimization for Compound-specific*
793 *Nitrogen Isotope Analysis of Amino Acids by Gas Chromatography/*
794 *Combustion/Isotope Ratio Mass Spectrometry in Earth, Life and Isotopes*
795 (eds. Ohkouchi, N. *et al.*) 367–386 (Kyoto University Press, 2010).
- 796 55. Bolger, A. M., Lohse, M. & Usadel, B. Trimmomatic: a flexible trimmer for
797 Illumina sequence data. *Bioinformatics* **30**, 2114–2120 (2014).
- 798 56. Leggett, R. M., Clavijo, B. J., Clissold, L., Clark, M. D. & Caccamo, M.
799 NextClip: an analysis and read preparation tool for Nextera Long Mate Pair
800 libraries. *Bioinformatics* **30**, 566–568 (2014).
- 801 57. Bankevich, A. *et al.* SPAdes: A new genome assembly algorithm and its
802 applications to single-cell sequencing. *J. Comput. Biol.* **19**, 455–477 (2012).
- 803 58. Lin, H.-H. & Liao, Y.-C. Accurate binning of metagenomic contigs via
804 automated clustering sequences using information of genomic signatures and
805 marker genes. *Sci. Rep.* **6**, 24175 (2016)
- 806 59. Boetzer, M., Henkel, C. V., Jansen, H. J., Butler, D. & Pirovano, W.
807 Scaffolding pre-assembled contigs using SSPACE. *Bioinformatics* **27**, 578–
808 579 (2011).
- 809 60. Seemann, T. Prokka: rapid prokaryotic genome annotation. *Bioinformatics*
810 **30**, 2068–2069 (2014).
- 811 61. Marchler-Bauer, A. & Bryant, S. H. CD-Search: protein domain annotations
812 on the fly. *Nucleic Acids Res.* **32**, W327–W331 (2004).
- 813 62. Marchler-Bauer, A. *et al.* CDD: NCBI's conserved domain database. *Nucleic*
814 *Acids Res.* **43**, D222–226 (2015).
- 815 63. Petersen, T. N., Brunak, S., Heijne, von, G. & Nielsen, H. SignalP 4.0:
816 discriminating signal peptides from transmembrane regions. *Nat. Meth.* **8**,
817 785–786 (2011).
- 818 64. Yin, Y. *et al.* dbCAN: a web resource for automated carbohydrate-active
819 enzyme annotation. *Nucleic Acids Res.* **40**, W445–W451 (2012).
- 820 65. Rawlings, N. D., Barrett, A. J. & Finn, R. Twenty years of the MEROPS

- database of proteolytic enzymes, their substrates and inhibitors. *Nucleic Acids Res.* **44**, D343–D350 (2016).

66. Fischer, M. & Pleiss, J. The lipase engineering database: a navigation and analysis tool for protein families. *Nucleic Acids Res.* **31**, 319–321 (2003).

67. Søndergaard, D., Pedersen, C. N. S. & Greening, C. HydDB: A web tool for hydrogenase classification and analysis. *Sci. Rep.* **6**, 34212 (2016).

68. Boutet, E., Lieberherr, D., Tognolli, M., Schneider, M. & Bairoch, A. UniProtKB/Swiss-Prot. *Methods Mol. Biol.* **406**, 89–112 (2007).

69. Lima, T. *et al.* HAMAP: a database of completely sequenced microbial proteome sets and manually curated microbial protein families in UniProtKB/Swiss-Prot. *Nucleic Acids Res.* **37**, D471–D478 (2009).

70. Katoh, K. & Standley, D. M. MAFFT multiple sequence alignment software version 7: improvements in performance and usability. *Mol. Biol. Evol.* **30**, 772–780 (2013).

71. Kozlov, A. M., Darriba, D., Flouri, T., Morel, B. & Stamatakis, A. RAxML-NG: A fast, scalable, and user-friendly tool for maximum likelihood phylogenetic inference. *Bioinformatics* (2019). in press.

72. Pruesse, E., Peplies, J. & Glöckner, F. O. SINA: Accurate high-throughput multiple sequence alignment of ribosomal RNA genes. *Bioinformatics* **28**, 1823–1829 (2012).

73. Quast, C. *et al.* The SILVA ribosomal RNA gene database project: improved data processing and web-based tools. *Nucleic Acids Res.* **41**, D590–D596 (2013).

74. Stamatakis, A. RAxML version 8: a tool for phylogenetic analysis and post-analysis of large phylogenies. *Bioinformatics* **30**, 1312–1313 (2014).

75. Capella-Gutiérrez, S., Silla-Martínez, J. M. & Gabaldón, T. trimAl: a tool for automated alignment trimming in large-scale phylogenetic analyses. *Bioinformatics* **25**, 1972–1973 (2009).

76. Price, M. N., Dehal, P. S. & Arkin, A. P. FastTree 2—approximately maximum-likelihood trees for large alignments. *PLoS ONE* **5**, e9490 (2010).

77. Magoc, T., Wood, D. & Salzberg, S. L. EDGE-pro: estimated degree of gene expression in prokaryotic genomes. *Evol. Bioinform. Online* **9**, 127–136 (2013).

- 854 78. Axley, M. J. & Grahame, D. A. Kinetics for formate dehydrogenase of
855 *Escherichia coli* formate-hydrogenlyase. *J. Biol. Chem.* **266**, 13731–13736
856 (1991).
- 857 79. Itoh, T., Suzuki, K.-I. & Nakase, T. *Thermocladium modestius* gen. nov., sp.
858 nov., a new genus of rod-shaped, extremely thermophilic crenarchaeote. *Int.*
859 *J. Syst. Bacteriol.* **48**, 879–887 (1998).
- 860 80. Zillig, W. *et al.* The archaeabacterium *Thermofilum pendens* represents, a
861 novel genus of the thermophilic, anaerobic sulfur respiring *Thermoproteales*.
862 *Syst. Appl. Microbiol.* **4**, 79–87 (1983).

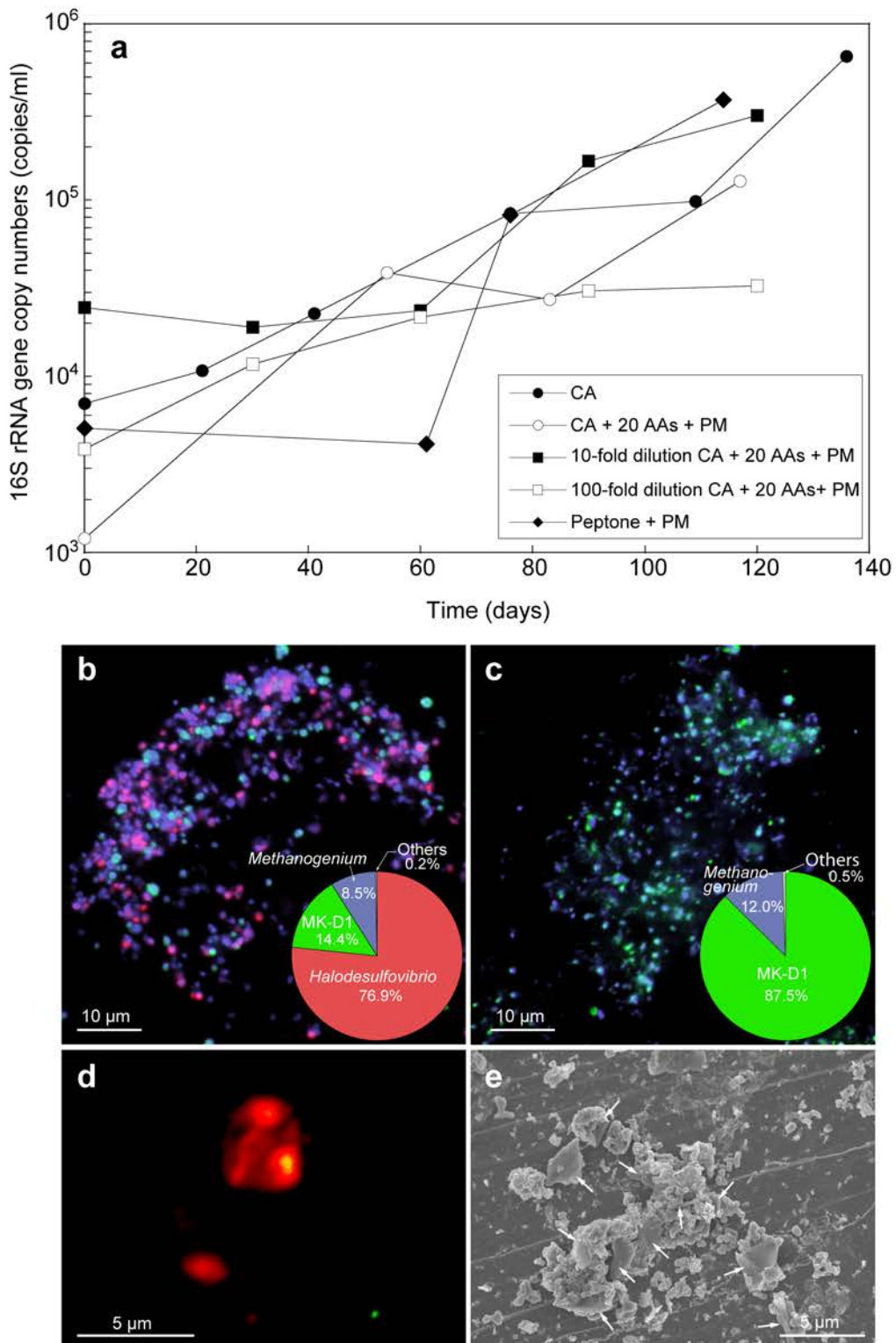


Fig. 1 | Growth curves and photomicrographs of the cultured Lokiarchaeota strain MK-D1. a, Growth curves of MK-D1 in anaerobic media supplemented with Casamino acids (CA; 0.05%, w/v) alone; CA with 20 amino acids (20 AAs; 0.1 mM of each) and powdered milk (PM; 0.1%, w/v); or peptone (0.1%, w/v) with PM. Results are also shown for cultures fed with 10- and 100-fold dilution of CA, 20 AAs, and PM. **b, c,** Fluorescence images of cells from enrichment cultures after eight (b) and eleven (c) transfers stained with DAPI (violet) and hybridized with nucleotide probes targeting MK-D1 (green) and *Bacteria* (red). Pie charts show relative abundance of microbial populations based on SSU rRNA gene tag-sequencing (iTAG) analysis. **d,** A fluorescence image of cells from enrichment cultures after eleven transfers hybridized with nucleotide probes targeting MK-D1 (green) and *Methanogenium* (red). **e,** SEM image of a highly purified co-culture of MK-D1 and *Methanogenium*. White arrows indicate *Methanogenium* cells. The detailed iTAG-based community compositions of cultures corresponding to each of the images are shown in Supplementary Table S2.

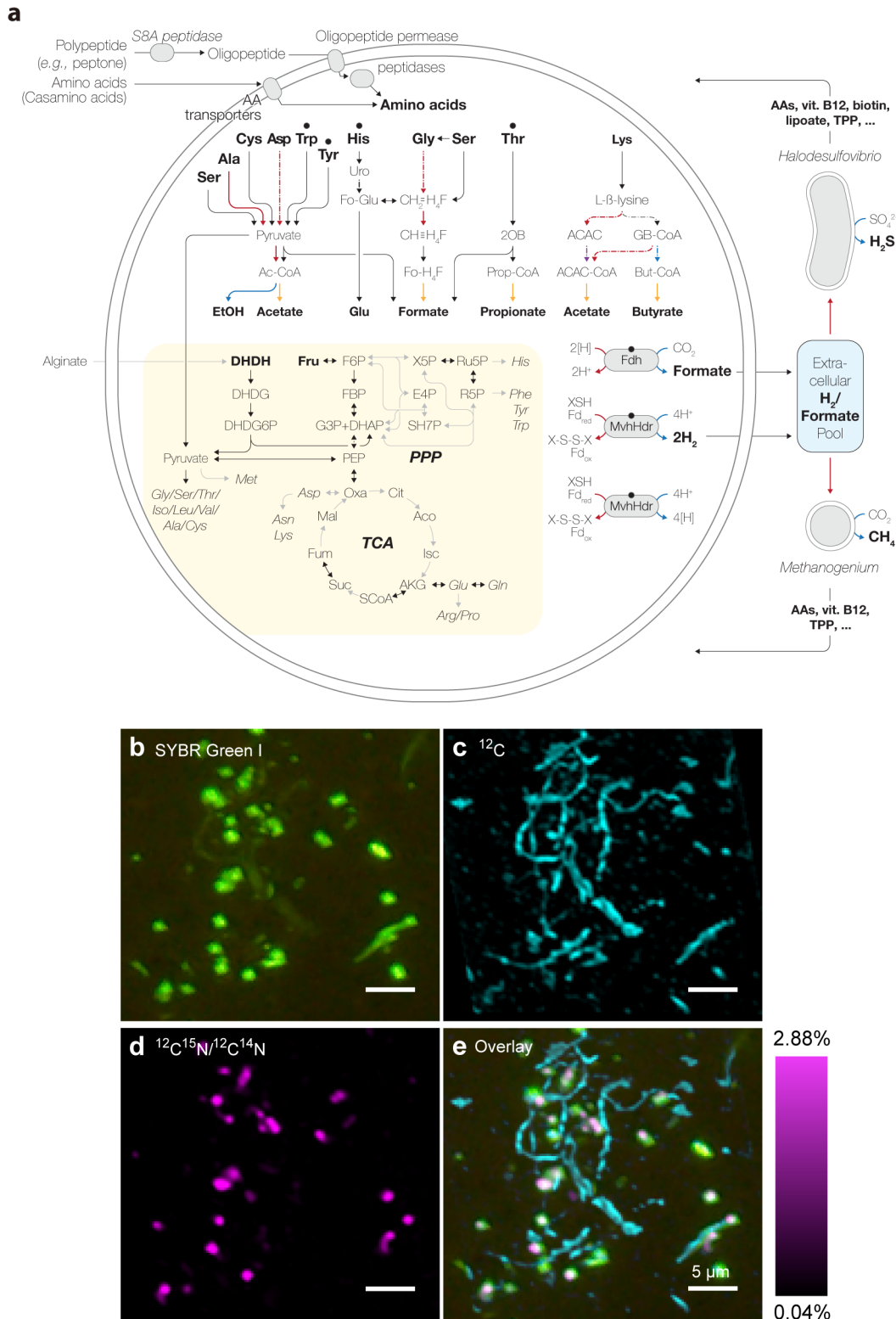


Fig. 2 | Syntrophic amino acid utilization of MK-D1. a, Genome-based metabolic reconstruction of MK-D1. Metabolic pathways identified (colored or black) and not identified (gray) are shown. For identified pathways, each step (solid line) or process (dotted) is marked by whether it is oxidative (red), reductive (blue), ATP-yielding (orange), or ATP-consuming (purple). Wavy arrows indicate exchange of compounds: formate, H_2 , AAs, vitamin B12, biotin, lipoate, and thiamine pyrophosphate (tpp) which are predicted to be metabolized or synthesized by the partnering *Halodesulfovibrio* and/or *Methanogenium*. Biosynthetic pathways are indicated with a yellow background. Metatranscriptomics-detected AA-catabolizing pathways are indicated (black dots above AAs). Abbreviations: 4,5-dihydroxy-2,6-dioxohexanoate (DHDH), 2-dehydro-3-deoxy-D-gluconate (DHDG), 3-dehydro-3-deoxy-D-gluconate 6-phosphate (DHDG6P), acetyl-CoA (Ac-CoA), urocanate (uro), formyl glutamate (Fo-Glu), methylene-tetrahydrofolate ($\text{CH}_3=\text{H}_4\text{F}$), methenyl-tetrahydrofolate ($\text{CH}=\text{H}_4\text{F}$), formyl-tetrahydrofolate (Fo-H4F), 2-oxobutyrate (2OB), propionyl-CoA (Prop-CoA), acetoacetate (ACAC), gamma-amino-butyryl-CoA (GB-CoA), butyryl-CoA (But-CoA), ferredoxin (Fd), thiol/disulfide pair (XSH/X-S-S-X), tricarboxylic acid (TCA) cycle, and pentose-phosphate pathway (PPP). **b-e**, NanoSIMS analysis of a highly purified MK-D1 culture incubated with ^{13}C - and ^{15}N -labeled AA mixture. **b**, Green fluorescent micrograph of SYBR Green I-stained cells. Aggregates are MK-D1, and filamentous cells are *Methanobacterium* sp. strain MO-MB1 (fluorescence can be weak due to high rigidity and low permeability of cell membrane [Supplementary Fig. S1]). **c**, NanoSIMS ion image of ^{12}C (cyan). **d**, NanoSIMS ion image of $^{12}\text{C}^{15}\text{N}/^{12}\text{C}^{14}\text{N}$ (magenta). **e**, Overlay image of **b-d**. The right-hand scale bar indicates the relative abundance of ^{15}N expressed as $^{15}\text{N}/^{14}\text{N}$. The iTAG analysis of the imaged culture is shown in Supplementary Table S2.

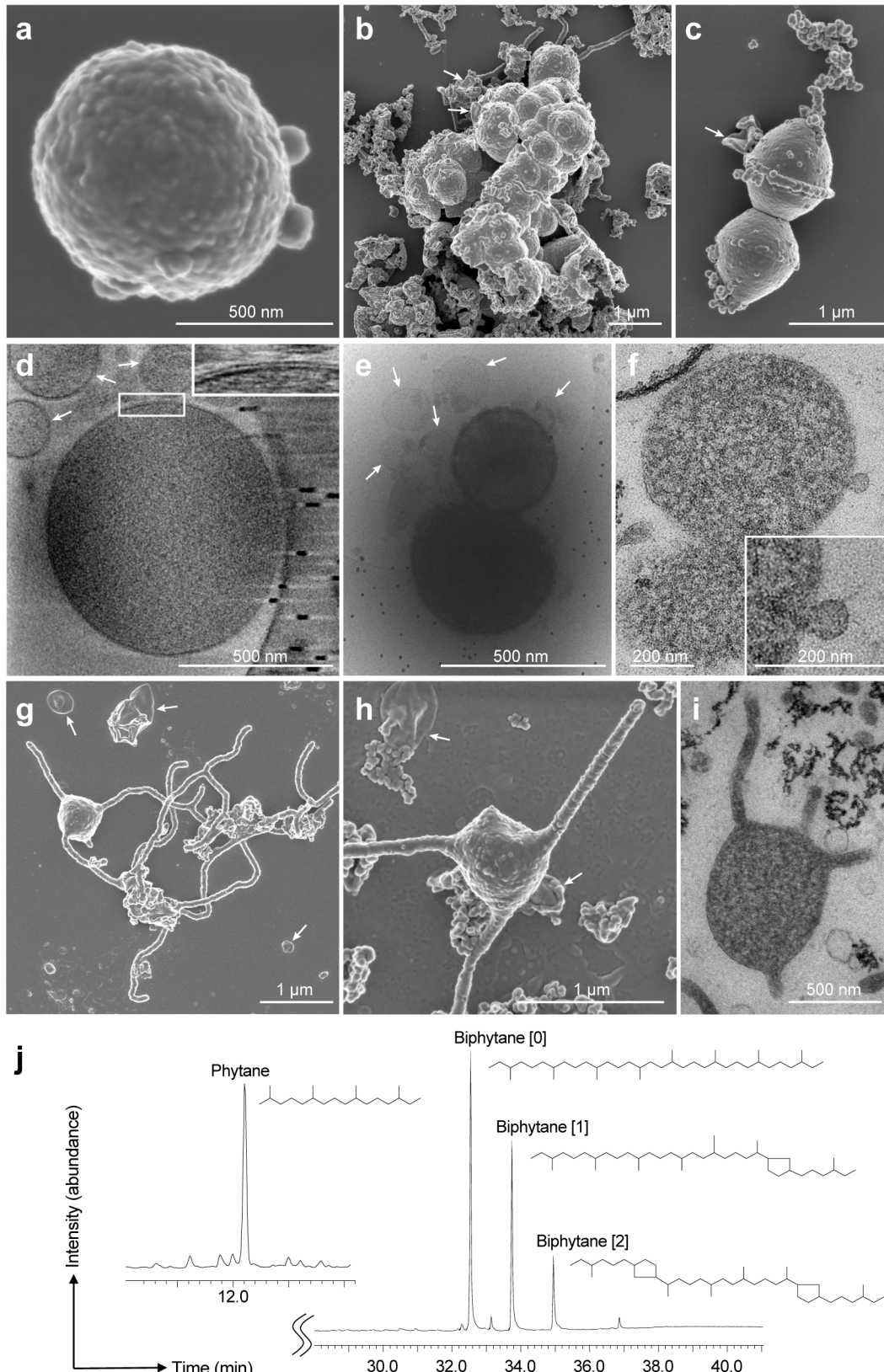
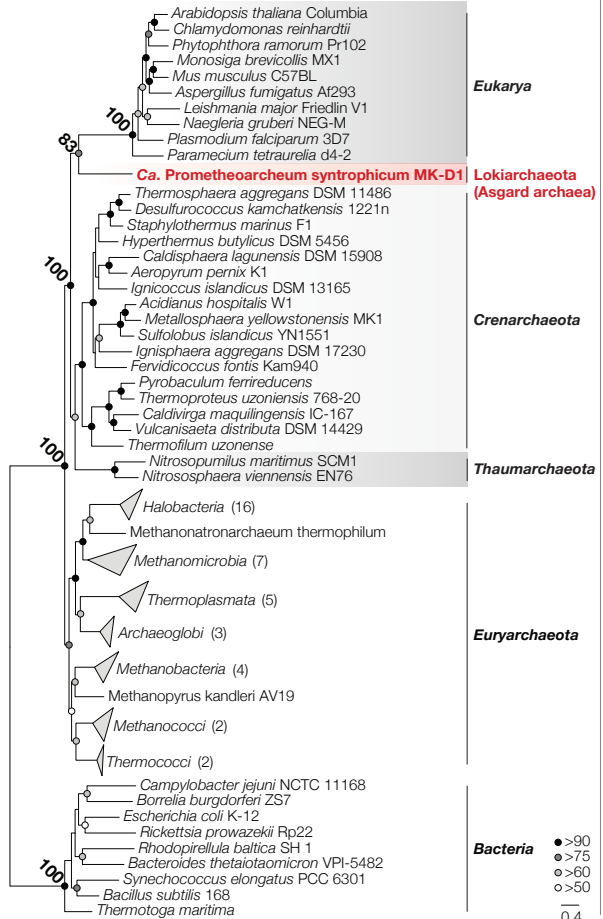


Fig. 3 | Microscopic characterization and lipid composition of MK-D1. **a–c**, SEM images of MK-D1. Single cell (**a**), aggregated cells covered with EPS-like materials (**b**), and a dividing cell with polar chains of blebs (**c**). **d**, Cryo-electron tomography image of MK-D1. The upper-right inset image shows a close-up of the boxed area for showing cell envelope structure. **e**, Cryo-electron microscopy (EM) image of large MVs attached and surrounding MK-D1 cells. **f**, Ultrathin section of an MK-D1 cell and an MV. The lower-right inset image shows a magnified view of the MV. **g, h**, SEM images of MK-D1 cells producing long branching (**g**) and straight (**h**) membrane protrusions. **i**, Ultrathin section of a MK-D1 cell with protrusions. **j**, A total ion chromatogram of mass spectrometry for lipids extracted from a highly purified MK-D1 culture. The chemical structures of isoprenoid lipids are also shown (see also Supplementary Fig. S2). The experiment were repeated twice and gave similar results. White arrows in the images indicate large MVs. Detailed iTAG-based community compositions of the cultures are shown in Supplementary Table S2.

a



b

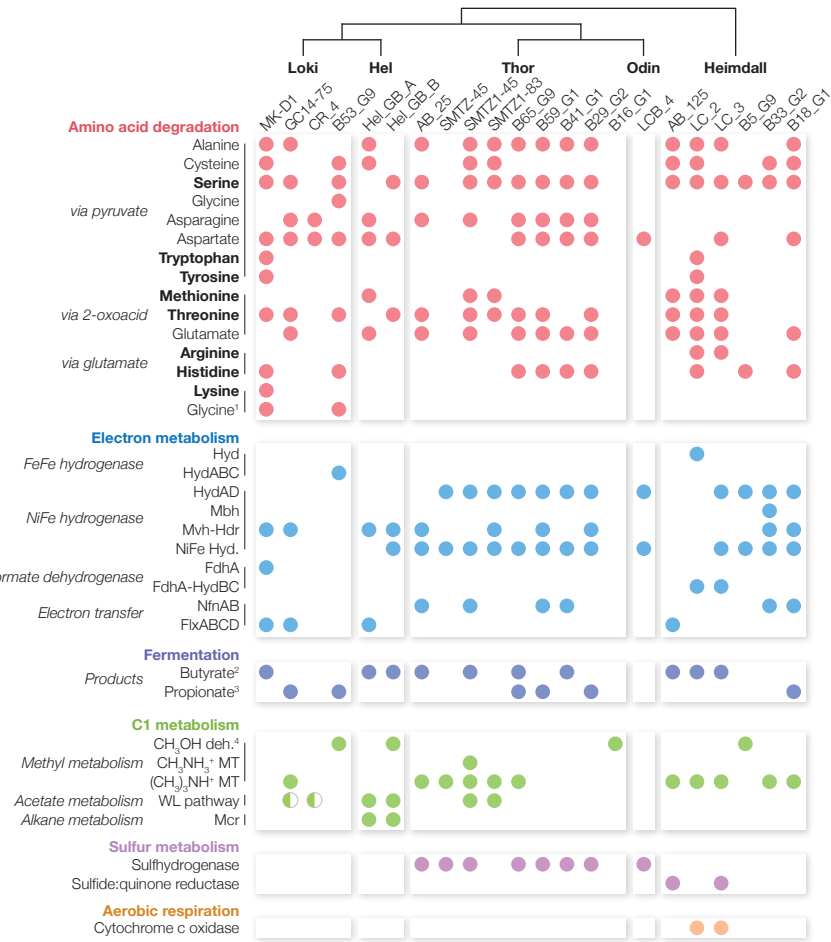


Fig. 4 | Phylogeny of MK-D1 and catabolic features of Asgard archaea. **a**, Phylogenomic tree of MK-D1 and select cultured archaea, eukaryotes, and bacteria based on 31 ribosomal proteins conserved across the three domains (Supplementary Table S4). Ribosomal protein sequences were collected from MK-D1 and other representative cultured organisms (Supplementary Table S5) and aligned individually using MAFFT (--linsi). After removing all-gap positions and concatenation, the maximum likelihood tree was constructed using RAxML-ng (fixed empirical substitution matrix [LG], 4 discrete GAMMA categories, empirical AA frequencies, and 100 bootstrap replicates). Bootstrap values around critical branching points are also shown. **b**, The presence/absence of AA degradation, electron metabolism, fermentation, C1 metabolism, sulfur metabolism, and aerobic respiration in individual genomes are shown (complete pathway – full circle; mostly complete pathway – half circle). For AA metabolism, pathways that are exclusively used for catabolism/degradation are bolded. ¹ Glycine metabolism through pyruvate (above) or formate (below). ² Butyrate metabolism is reversible (fermentation or beta oxidation), but the butyryl-CoA dehydrogenases tend to be associated with EtfAB in the genomes, suggesting formation of an electron-confurcating complex for butyrate fermentation. ³ Determined by presence of methylmalonyl-CoA decarboxylase, biotin carboxyl carrier protein, and pyruvate carboxylase. Propionate metabolism is also reversible, but no Asgard archaea member encodes the full set of genes necessary for syntrophic propionate degradation. ⁴ Alcohol dehydrogenases can have diverse substrate specificities. Abbreviations: monomeric FeFe hydrogenase (Hyd), trimeric electron-confurcating FeFe hydrogenase (HydABC), reversible NADPH-dependent NiFe hydrogenase (HydAD), reversible heterodisulfide-dependent electron-confurcating hydrogenase (Mvh-Hdr), other NiFe hydrogenases (NiFe Hyd.), formate dehydrogenase (FdHA), putative electron-confurcating formate dehydrogenase (FdhA-HydBC), NADH-dependent NADPH:ferredoxin oxidoreductase (NfnAB), heterodisulfide- and flavin-dependent oxidoreductase of unknown function (FlxABCD), tetrahydromethanopterin methyltransferase (MT), Wood-Ljungdahl (WL), and methyl-CoM reductase (Mcr).

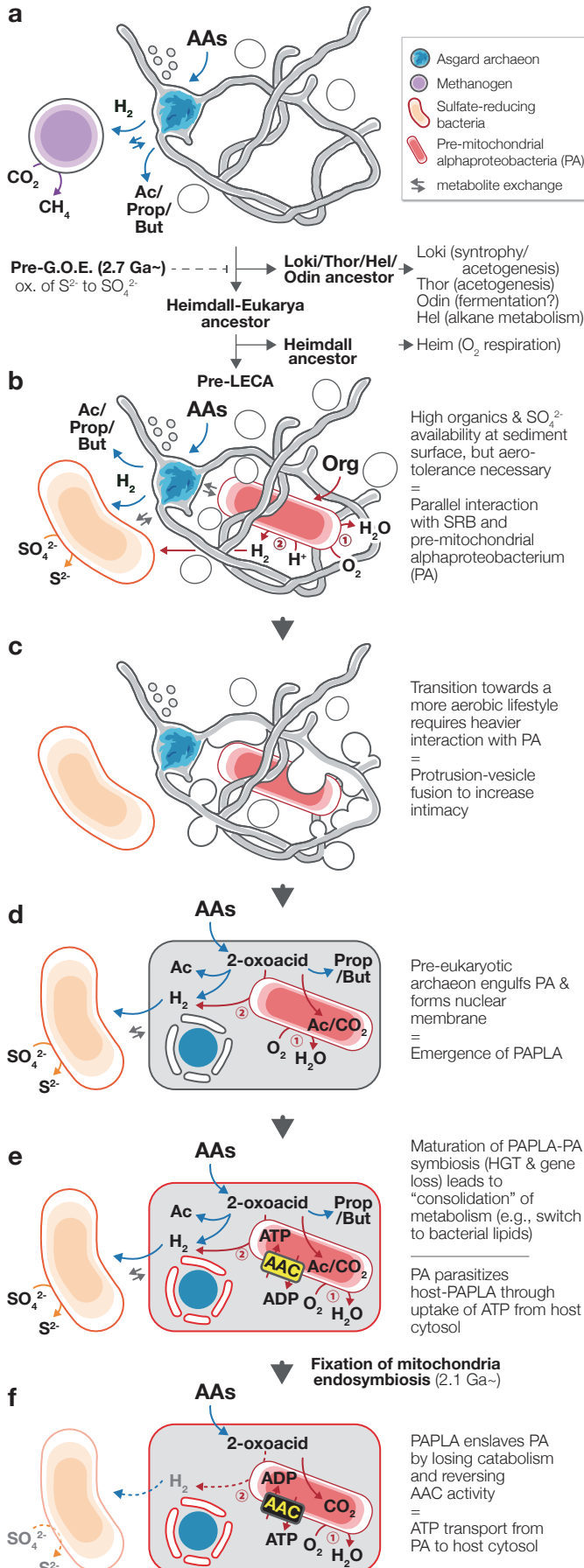


Fig. 5 | A new evolutionary model “Entange-Engulf-Enslave (E³)” for eukaryogenesis. **a**, Syntrophic/fermentative Asgard archaea ancestor likely degraded AAs to short-chain fatty acids and H₂. With the rising of Earth’s O₂ concentrations due to oxygenic photosynthesis (around the Great Oxidation Event [G.O.E.]), Asgard archaea diverged towards specialized anaerobic niches (Lokiarchaeta [Loki], Thorarchaeota [Thor], Odinarchaeota [Odin], and Helarchaeota [Hel]) and aerobiosis (Heimdallarchaeota [Heimdall] and Eukarya). **b**, To thrive at the oxic-anoxic interface with high organic and sulfate availability, pre-LECA (last eukaryote common ancestor) archaeon syntrophically interacted with H₂-scavenging SRB (orange) and O₂-scavenging organotrophic pre-mitochondrial alphaproteobacterium (PA; red). PA could likely degrade organics (1) aerobically or (2) anaerobically in interaction with SRB. Given the restricted biosynthetic capacities of all extant Asgard archaea, the pre-LECA archaeon necessitated metabolite exchange with SRB and PA. **c**, Protrusions and MVs tangle with PA and enhance physical interaction; protrusion-MV fusion mediates further intimate interactions, and ultimately leads to PA engulfment. This mechanism for engulfment allows for formation of a nucleoid-bounding membrane topologically similar to the eukaryote nuclear membrane. **d**, After engulfment, the pre-LECA archaeon and PA can continue the interaction shown in **(b)**, leading to emergence of a PA-containing pre-LECA archaeon (PAPLA) with primitive endosymbiosis. **e**, Maturation of PAPLA-PA symbiosis and development of PA parasitism. **f**, Enslavement of PA by PAPLA through delegation of ATP generating metabolism to PA.